# The Autocorrelation Spectral Density for Doppler-Weather-Radar Signal Analysis

David A. Warde, *Member, IEEE*, and Sebastián M. Torres, *Senior Member, IEEE*

***Abstract*—Time-domain autocovariance processing is widely accepted as a computationally efficient method to estimate the first three spectral moments of Doppler weather radar signals (i.e., mean signal power, mean Doppler velocity, and spectrum width). However, when signals with different frequency content (e.g., ground clutter) contaminate the weather signal, spectral processing using the periodogram estimator of the power spectral density (PSD) is the preferred tool of analysis. After spectral processing (i.e., filtering), a PSD-based autocorrelation estimator is typically employed to produce unbiased estimates of the weather-signal spectral moments. However, the PSD does not convey explicit phase information, which has the potential to aid in the spectral analysis of radar signals. In this paper, the autocorrelation spectral density (ASD) is introduced for spectral analysis of weather-radar signals as a generalization of the classical PSD, and an ASD-based autocorrelation estimator is proposed to produce unbiased estimates of the weather-signal spectral moments. A significant advantage of the ASD over the PSD is that it provides explicit phase information that can be exploited to identify and remove certain types of contaminant signals. Thus, the ASD provides an alternative means for spectral analysis, which can lead to improved quality of meteorological data from weather radars.**

***Index Terms*—Autocorrelation estimation, autocorrelation spectral density (ASD), clutter filtering, Doppler weather radar, signal processing, spectral analysis.**

## I. Introduction

REMOTE sensing of the atmosphere by Doppler weather radar relies on amplitude and frequency shifts of electromagnetic backscatter from distributed hydrometeors in the radar volume. The expected power spectral density (PSD) for weather echoes is Gaussian [1], and stochastic signal processing techniques are used to extract the first three moments (i.e., mean signal power, mean radial velocity, and spectrum width) from the digitized complex voltages of received radar echoes [2]. Traditionally, meteorological information is extracted in the time domain from estimates of the autocorrelation function at several small lags. That is, the magnitude of autocorrelation function at lag zero is the mean power of the signal from which the radar reflectivity is derived; the argument at lag-1 is proportional to the mean radial velocity; and, under the Gaussian-spectrum assumption, the ratio of magnitudes from two or more lags is used to estimate the spectrum width [3].

Often, weather signals are contaminated with undesired signals from non-meteorological sources such as the ground (e.g., man-made structures and terrain), biota (e.g., insects and birds), point targets (e.g., cars and airplanes), and electromagnetic interference (e.g., other radar systems). One of the main goals of weather-radar signal processing is to minimize contributions from these contaminants (generically referred to as clutter) so that unbiased meteorological data can be obtained and delivered to both human users and automatic algorithms. Spectral analysis based on the PSD provides a powerful and intuitive tool to separate clutter from weather signals [4]. In [5], the authors discuss the advantages of using spectral processing for ground clutter suppression and review several such techniques. Further, with the advent of modern signal processors capable of performing discrete Fourier transforms (DFT) in real time, spectral ground clutter filters [6] have been developed and implemented on operational systems. For example, the Weather-Surveillance-Radar-1988-Doppler (WSR-88D) signal processor was updated a few years ago to exploit spectral processing for the mitigation of ground clutter using the PSD [7]. Other techniques exploit different spectral representations; for example, the phase of the cross-spectrum of odd and even samples was recently proposed to identify ground clutter contamination [8]. Regardless of the means of identification, contaminated spectral components must be filtered for further processing as described next.

In a typical weather-radar signal-processing pipeline, once the non-meteorological contaminants are identified and removed, the filtered (uncontaminated) spectrum is used to estimate the autocorrelation function at a few small lags [9]. In the context of spectral processing, the autocorrelation function can be obtained as the inverse Fourier transform of the PSD [10], which assumes signal periodicity with period equal to the observation time (or dwell time). Such an assumption is unrealistic with finite observation times because weather signals contain a continuum of frequencies [11], which in theory require an infinitely long observation time to faithfully derive their PSD. Thus, PSD-based autocorrelation estimates at lags greater than zero must be made unbiased in both magnitude and phase. That is, the magnitude bias is removed by renormalization and the phase bias is removed by either zero padding or by subtracting the spurious terms arising from the implicit circular convolution in the inverse DFT [12].

A more significant limitation of the PSD is that it does not convey explicit phase information, which has the potential to aid in the spectral analysis of weather-radar signals by revealing

Manuscript received June 1, 2012; revised December 11, 2012; accepted January 15, 2013. Date of publication March 7, 2013; date of current version November 26, 2013. This work was supported by the National Oceanic and Atmospheric Administration (NOAA)/Office of Oceanic and Atmospheric Research under NOAA-University of Oklahoma Cooperative Agreement NA11OAR4320072, U.S. Department of Commerce.

The authors are with the Cooperative Institute for Mesoscale Meteorological Studies, The University of Oklahoma, and NOAA/OAR National Severe Storms Laboratory, Norman, OK 73072 USA (e-mail: david.a.warde@noaa.gov; sebastian.torres@noaa.gov).

Digital Object Identifier 10.1109/TGRS.2013.2241775

information not obvious in the magnitude. In this paper, the autocorrelation spectral density (ASD) is introduced for spectral analysis as a generalization of the classical PSD. It will be shown that the ASD is attractive for radar signal analysis for two reasons: 1) the ASD explicitly conveys phase information that is not obvious in the PSD, and 2) an autocorrelation estimator based on the ASD is equivalent to the classical time-domain, unbiased autocorrelation estimator. That is, unlike the PSD, the ASD leads to unbiased autocorrelation estimates at all lags without the usual (although invalid) periodicity assumption. Thus, the ASD provides an alternative means for spectral analysis of radar signals, which can lead to improved quality of meteorological data from weather radars.

The rest of the paper is organized as follows. In Section II, the ASD is defined and its interpretation for spectral analysis is provided. Section III introduces an ASD-based autocorrelation estimator, which is shown to be unbiased like the classical time-domain autocorrelation estimator. Spectral analysis using the ASD is described in Section IV, where spectral leakage effects on its argument are shown to provide a means to identify the spectral extent to narrowband contaminants. Section V presents two examples using the lag-1 ASD that illustrate such identification using ground-clutter and point-target contaminants. Finally, Section VI concludes this work with recommendations for using the ASD for spectral analysis of weather-radar signals.

## II. Autocorrelation Spectral Density

The ASD can be regarded as a generalization of the classical PSD; however, unlike the PSD, the ASD includes explicit phase information, which can be exploited for spectral analysis of radar signals. The lag-$l$ ASD estimator is defined as an extension of the PSD estimator based on the modified periodogram [13]. That is

$$\hat{S}_l(f) = \frac{T_s}{M-l} F_0^*(f) F_l(f), \quad \text{for } -(2T_s)^{-1} < f < (2T_s)^{-1} \tag{2.1}$$

where $f$ is Doppler frequency, a "hat" is used to indicate an estimated quantity, $*$ denotes complex conjugate, $l$ is the lag (a positive integer), $M$ is the number of samples in the dwell time, and $T_s$ is the pulse repetition time (i.e., the sampling period for the time-series data). The ASD should not be confused with the Fourier transform of the autocorrelation function, which is merely the PSD; however, the lag-0 ASD is in fact the PSD. Whereas estimating the PSD involves only one Fourier transform, the ASD estimator for lags other than zero requires two: one for $F_0$ and one for $F_l$. Here, $F_l$ is the discrete-time Fourier transform (DTFT) of the time-shifted, $(M-l)$-sample time series after windowing. That is

$$F_l(f) = \sum_{m=-\infty}^{\infty} d(m) V(m+l) e^{-j2\pi f T_s m} \tag{2.2}$$

where $V(m)$ is the complex time series, and $d$ is the data window. The data window is real valued function, symmetric about $(M-l-1)/2$, normalized for average unit power, and takes zero values outside the interval $[0, M-l-1]$; thus, the limits of the summation in (2.2) can be adjusted to get

$$F_l(f) = \sum_{m=0}^{M-l-1} d(m) V(m+l) e^{-j2\pi f T_s m}. \tag{2.3}$$

Note that $F_l$ is periodic with period $T_s^{-1}$; moreover, $F_0$ is the DTFT of the original (nonshifted) time series after windowing. For a given lag $l$, both complex spectra, $F_0$ and $F_l$, are estimated using the same number of samples, $M-l$, with a power-preserving data window of the same length.

In Appendix A, the expected value of the lag-$l$ ASD estimator is derived as

$$E\left[\hat{S}_l(f)\right] = \left[S(f) e^{j2\pi f T_s l}\right] \circledast W(f) \tag{2.4}$$

where $\circledast$ denotes circular convolution, and $W$ is the DTFT of the lag window $w$, which in turn depends on the data window $d$ (Appendix A). As derived in Appendix A, the variance of the lag-$l$ ASD estimator is the same as the variance of the PSD. Further, in the limit for an infinitely large data set, the windowing effects on the ASD estimator vanish since $\lim_{M\to\infty} W(f) = \delta(f)$, where $\delta(f)$ is the Dirac delta function, and the expected lag-$l$ ASD becomes

$$\lim_{M\to\infty} E\left[\hat{S}_l(f)\right] = S(f) e^{j2\pi f T_s l} \tag{2.5}$$

with a variance of

$$\lim_{M\to\infty} Var\left[\hat{S}_l(f)\right] = S^2(f). \tag{2.6}$$

Hence, for an infinite data set, the ASD is trivial: its magnitude is the well-known PSD and its phase is linear with slope proportional to $l$. However, in the presence of windowing effects for the typical numbers of samples employed on operational weather radars, the phase of the ASD is not trivial and, as will be illustrated later, provides additional information. Thus, the ASD can be thought of as an alternative tool for spectral analysis of radar signals.

## III. Autocorrelation Estimation Based on the ASD

Doppler weather radars usually provide estimates of meteorological variables obtained from autocorrelation estimates $\hat{R}(lT_s)$ at a few small lags. For example, mean signal power, mean Doppler velocity, and spectrum width can be estimated as [11]

$$\hat{S} = \hat{R}(0) - N \tag{3.1}$$

$$\hat{v} = -\frac{v_a}{\pi} \arg\left[\hat{R}(T_s)\right] \tag{3.2}$$

$$\hat{\sigma}_v = \frac{v_a\sqrt{2}}{\pi} \sqrt{\left| \ln\left( \frac{\hat{R}(0) - N}{\left|\hat{R}(T_s)\right|} \right) \right|} \tag{3.3}$$

respectively, where $N$ is the receiver noise power and $v_a$ is the Nyquist velocity. Thus, autocorrelation estimation is at the core of most weather-radar signal processors. This section

reviews the typical time-domain autocorrelation estimator and introduces a new one based on the ASD.

For a set of $M$ complex samples $V$, the time-domain unbiased autocorrelation estimator at lag $l$ ($T_s$ is dropped for simplicity) is given as

$$\hat{R}_{UNB}(l)=\frac{1}{M-l}\sum_{m=0}^{M-l-1}V^*(m)V(m+l), \qquad \text{for } 0\le l<M. \tag{3.4}$$

This estimator is computationally simple, its statistical performance is well understood (e.g., [14]), and it is typically used for meteorological-variable estimators in the time domain. It is straightforward to show that it is unbiased by taking the expected value of the previous equation:

$$\begin{aligned} E\left[\hat{R}_{UNB}(l)\right] &= \frac{1}{M-l}\sum_{m=0}^{M-l-1}E\left[V^*(m)V(m+l)\right] \\ &= \frac{1}{M-l}\sum_{m=0}^{M-l-1}R(l)=R(l) \end{aligned} \tag{3.5}$$

where we used the definition of the autocorrelation in [11].

A new autocorrelation estimator can be derived from the ASD as

$$\hat{R}_{ASD}(l)=\frac{1}{(M-l)T_s}\sum_{k=0}^{M-l-1}\hat{S}_l(k) \tag{3.6}$$

where $\hat{S}_l$ is the lag-$l$ ASD estimator given in (2.1). It can be shown that for a rectangular data window, the unbiased and ASD-based autocorrelation estimators are identical (Appendix B); thus, they share the same statistical properties. However, for tapered data windows, the ASD-based autocorrelation estimator is unbiased only if the data window is purposely scaled to be power preserving. Appendix B provides a formal derivation of the ASD-based autocorrelation estimator bias and variance.

## IV. Spectral Analysis Using the ASD

Having introduced the ASD as a generalization of the PSD and shown that the ASD-based autocorrelation estimator is unbiased when using a properly normalized data window, we now address the usefulness of the ASD for spectral analysis. Based on (2.5), it would seem that the phase of the ASD is trivial and does not carry any useful information. However, it will be shown next that, for finite sample sets, the phase biases in the ASD result from spectral leakage and provide information not obvious in the PSD.

Weather signals at the radar receiver are the composite of a very large number of hydrometeor echoes in the radar resolution volume. Thus, they can be decomposed as individual contributions of complex sinusoids (cf. [11, (4.1)]). In the following, we begin by analyzing the spectral leakage in the phase of the ASD of an elemental complex sinusoid (i.e., the backscatter from a single hydrometeor) and then generalize the results to composite signals (i.e., the composite backscatter from a large number of hydrometeors).

Consider an elemental, $M$-sample, discrete-time, complex sinusoidal signal defined as

$$V(m)=A_i e^{j(2\pi\alpha_i f_0 m T_s+\phi)}=A_i e^{j\left(\frac{2\pi\alpha_i m}{M-l}+\phi\right)}, \qquad 0\le m<M \tag{4.1}$$

where $A_i$ is the signal amplitude, $\alpha_i f_0$ is its frequency, and $\phi$ is an arbitrary initial phase. Here, $\alpha_i$ is a real number and $f_0=1/(M-l)T_s$ is the fundamental analysis frequency of the DFTs in the lag-$l$ ASD estimator. The lag-$l$ ASD of this signal can be estimated from (2.1); using a rectangular data window, the complex spectra $F_0$ and $F_l$ are

$$F_0(k)=A_i e^{j\phi}\sum_{m=0}^{M-l-1}e^{j2\pi m\left(\frac{\alpha_i-k}{M-l}\right)}, \qquad 0\le k<M-l \tag{4.2}$$

and

$$F_l(k)=A_i e^{j\phi}e^{j\frac{2\pi\alpha_i l}{M-l}}\sum_{m=0}^{M-l-1}e^{j2\pi m\left(\frac{\alpha_i-k}{M-l}\right)}, \qquad 0\le k<M-l. \tag{4.3}$$

The sum of complex exponentials in the previous two equations can be expressed as

$$\sum_{m=0}^{M-l-1}e^{j2\pi m\left(\frac{\alpha_i-k}{M-l}\right)} = \begin{cases} (M-l)\Delta_{M-l}(\alpha_i-k) & \alpha\in\mathbb{Z} \\ e^{j\pi\frac{(M-l-1)}{M-l}(\alpha_i-k)}\dfrac{\sin[\pi(\alpha_i-k)]}{\sin\left[\frac{\pi(\alpha_i-k)}{M-l}\right]} & \alpha\notin\mathbb{Z} \end{cases} \tag{4.4}$$

where $\Delta_{M-l}$ is the Kronecker comb with period $M-l$, and $\mathbb{Z}$ is the set of integer numbers. The top term on the right-hand side of (4.4) corresponds to sinusoids with an integer number of cycles in $(M-l)T_s$. In this case, $F_0$ and $F_l$ are nonzero only for a single coefficient: $k=\alpha_i \bmod (M-l)$, which indicates the absence of spectral leakage. The bottom term on the right-hand side of (4.4) quantifies the effects of spectral leakage for all other complex sinusoids, a more interesting case in the context of our application. In this case, the lag-$l$ ASD estimate of the elemental signal is

$$\hat{S}_l^{(i)}(k)=T_s A_i^2 e^{j\frac{2\pi\alpha_i l}{M-l}}\Phi_{M-l}(k-\alpha_i) \tag{4.5}$$

where the superscript $(i)$ is used to denote the *i-th* elemental signal and $\Phi_{M-l}$ is the $(M-l)$-periodic Fejér kernel [15] given by

$$\Phi_{M-l}(k-\alpha_i)=\frac{1}{M-l}\frac{\sin^2\left[\pi(k-\alpha_i)\right]}{\sin^2\left[\frac{\pi(k-\alpha_i)}{M-l}\right]}. \tag{4.6}$$

Note that the Fejér kernel is the power spectrum of the rectangular data window of length $M-l$ and imparts no phase bias because it has real coefficients; thus, the phase bias from spectral leakage is given by

$$\Delta\phi(k)=2\pi l\left(\frac{\alpha_i-k}{M-l}\right) \tag{4.7}$$

where the expected phase of the lag-$l$ ASD is $2\pi lk/(M-l)$ [cf. (2.5)]. Because the phase of (4.5) is constant for all $k$, the

absolute value of the sum of the lag-$l$ ASD and the sum of its absolute values are equal to the mean power of the signal; i.e.,

$$\left|\frac{1}{T_s}\sum_{k=0}^{M-l-1}\hat{S}_l^{(i)}(k)\right| = \frac{1}{T_s}\sum_{k=0}^{M-l-1}\left|\hat{S}_l^{(i)}(k)\right| = A_i^2 \qquad (4.8)$$

where we used the fact that the sum of one period of the Fejér kernel is one. From this equation, we can infer that a complex sinusoid with frequency $\alpha_i f_0$ is "coherently spread" across the Nyquist co-interval in the ASD.

Equation (4.5) quantifies the contribution of the elemental signal in (4.1) to the $k$-th spectral coefficient of the lag-$l$ ASD. By superposition, $\hat{S}_l(k)$ for a composite signal is given by the sum of contributions from these elemental signals. Hence, the estimated ASD of the composite signal can be viewed as a convolution of its true ASD with the $(M-l)$-periodic power spectrum of a data window $(W_{M-l})$ as

$$\hat{S}_l(k) = \sum_i \hat{S}_l^{(i)}(k) = \sum_i T_s A_i^2 e^{j\frac{2\pi\alpha_i l}{M-l}} W_{M-l}(k-\alpha_i) \qquad (4.9)$$

where $W_{M-l}$ has been generalized as the power spectrum of any power-preserving data window with $M-l$ samples. Not surprisingly, (4.9) has the same form as (2.4). It should be noted that $W_{M-l}$ is a positive real function; consequently, the total bias in the phase of the ASD comes from the complex sum of elemental-signal contributions weighted by $W_{M-l}$. Explicitly, (4.9) confirms that the amount of spectral leakage is dependent on both the data window and the sample size, which is a well-known fact. Hence, as expected, the spectral leakage in the ASD estimate can be mitigated by using tapered data windows and/or more samples. Three characteristics of $W_{M-l}$ that account for the amount of spectral leakage experienced at each coefficient of the ASD are 1) the main-lobe width, 2) the first sidelobe level, and 3) the asymptotic falloff rate of the higher order sidelobes. Using data windows with low sidelobe levels reduces the biases away from the spectral peaks of the signal under analysis (i.e., helps contain spectral leakage), but this is usually accompanied by a wider main lobe, which results in increased localized biases around the spectral peaks (i.e., decreased spectral resolution). Thus, the selection of a data window entails finding a balance between spectral resolution and leakage. The reader is referred to [16] and [17] for details on many data windows commonly used in spectral analysis, and to [11, Fig. 5.9] which summarizes the relationship between the data window and its power spectrum.

It will be shown next that the biases seen in the ASD estimator are related to the spectral power gradient of the signal under analysis; that is, signals that have narrow spectrum (i.e., large spectral power gradient) induce larger localized biases than signals that have wide spectrum (i.e., small spectral power gradient). The elemental signal discussed above is an extreme for narrowband signals. For this signal, the ASD is biased in magnitude by the power spectrum of the data window and in phase by the expression in (4.7); thus, the largest biases are localized around the frequency of the elemental signal. On the other hand, an extreme for wideband signals is a composite signal made out of a large number of elemental signals with equal power and frequencies spanning the entire Nyquist co-interval (e.g., white noise). From (4.9), it is easy to show that

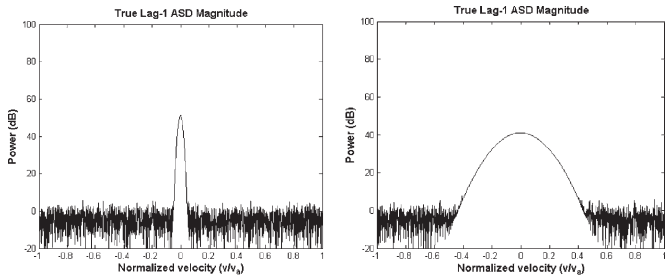


Fig. 1. PSD of Gaussian narrowband (left) and wideband (right) signals in additive white noise. For both signals, the SNR is 50 dB and the mean Doppler velocity is 0.

the ASD of this wideband signal is not biased when using a power-preserving data window. For signals with finite spectrum widths, the biases in the ASD will be in between the two extremes discussed above. That is, the ASD of narrowband signals will have biases similar to those from an elemental signal, and the ASD of wideband signals will be nearly unbiased. In all cases, the use of tapered windows will help to localize these biases around the spectral peaks of the signal while reducing the biases away from them.

Analogous to analyzing signals with the PSD, when mixed signals (e.g., a combination of weather signal, clutter, and noise) are analyzed with the ASD, the dominant signal may dictate the observed magnitude and phase at each spectral coefficient. For example, in a mixture of weather signal and noise, the ASD bias in a spectral coefficient away from the weather signal peak (i.e., a coefficient where noise is dominant) will be controlled by the larger of the noise power and the spectral leakage from the weather signal at that coefficient.

Examples of deterministic narrowband and wideband Gaussian signals with additive white noise are analyzed next. Although these are not realistic weather signals, they serve the purpose to illustrate the effects of spectral leakage described above. Fig. 1 shows the PSD of these signals using a very large sample set $(M = 2,049)$, which should approximate the true PSD. Each of these signals has a signal-to-noise ratio (SNR) of 50 dB and zero mean Doppler velocity. For this case, the Nyquist velocity is 30 m/s, which is typical of operational weather radars. The narrowband signal has a spectrum width of 0.3 m/s, which is representative of ground clutter [18]; and the wideband signal has a spectrum width of 3 m/s, which is representative of a weather signal [19]. Lag-1 ASD estimates for these signals with a sample size of $M = 64$ are shown in Fig. 2; panel $a$ shows the narrowband signal (magnitude on top and phase on bottom) while panel $b$ shows the same for the wideband signal. With an SNR of 50 dB, the strong spectral leakage from the rectangular window sidelobe levels ($\sim$13 dB below the peak) easily masks the noise. In this case, the measured phase of the lag-1 ASD is dominated by the signal spreading across the entire Nyquist co-interval; spectral leakage is so severe that biases are significant even for spectral coefficients far removed from the spectral peak of the signal. Note that this spectral leakage would completely obscure any other signal with an SNR less than $\sim$11 dB no matter how far away it were from the dominant peak. The magnitude of the ASD away from the spectral peak of the signal (i.e., where the true spectrum falls below the noise level) follows the asymptotic behavior of the

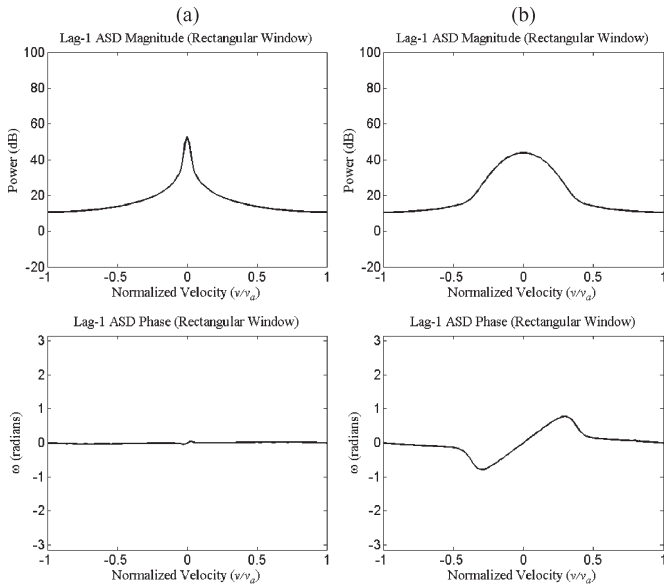


Fig. 2. Magnitude (top panels) and phase (bottom panels) of the lag-1 ASD using a rectangular data window for the narrowband signal (left panels), and wideband signal (right panels) in Fig. 1. (a) Narrowband; (b) wideband.

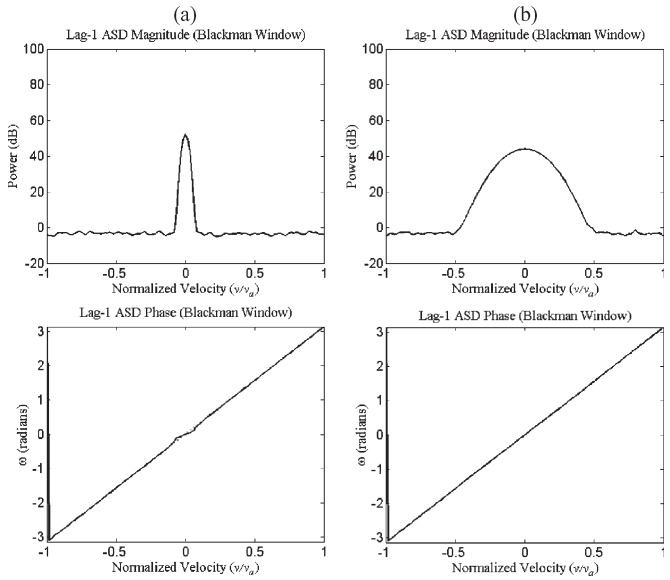


Fig. 3. Same as Fig. 2 but with a Blackman window. (a) Narrowband; (b) wideband.

rectangular-window power spectrum. Additionally, the phase of the ASD is dictated by the spectral extent of the signal, with the maximum phase bias occurring where the magnitude of the signal spectrum is just above the noise level.

As mentioned before, the use of tapered data windows can reduce the biases induced by spectral leakage observed in Fig. 2. A data window with a power spectrum that has sidelobe levels at or below 50 dB (the SNR of the signals in Fig. 1) is required to effectively contain spectral leakage. The Blackman window with a $-58$ dB first sidelobe level and a $-18$ dB/octave sidelobe falloff rate should be sufficient to contain the spectral leakage for these examples. Shown in Fig. 3 are the same plots as in Fig. 2 except that the Blackman window was applied. Unlike the biases shown in Fig. 2, neither magnitude nor phase biases are observed away from the spectral peak using the Blackman window; however, a broadening of the spectrum is evident. The ASD of the narrowband signal has a flattened phase localized around the spectral peak of the signal due to the high power gradient, whereas the ASD phases of the wideband signal appear nearly unbiased due to the small power gradient.

Although the spectral leakage is substantially reduced through the use of a tapered data widow, this results in an increased variance of ASD-based autocorrelation estimates due to the reduced weighting that the end samples receive. It should be noted that if only one signal were present (Fig. 1), it would be unnecessary to contain the spectral leakage. In this case, the ASD-based autocorrelation estimator using a rectangular window would be preferred as it would lead to the lowest variance of meteorological-variable estimates. However, in the context of weather-radar signal processing, spectral analysis is typically used to separate multiple signals (e.g., a weather signal from ground clutter). In this case, if the spectral leakage were not effectively contained, the biases in the ASD estimate would be evident on spectral components away from the spectral peak of the dominant signal (as in the case shown in Fig. 2 for the rectangular window). Alternatively, when the spectral leakage is effectively contained (e.g., using the Blackman window as in Fig. 3), the ASD is biased only in the vicinity of the spectral peak of the dominant signal, and narrowband signals lead to more pronounced biases than wideband signal. Thus, the value of the ASD as a tool for spectral analysis lies in the fact that biases arising from spectral leakage are very clearly depicted in the phase of the ASD. This important property is demonstrated next.

A comparison of PSD and lag-1 ASD analyses of real data can highlight the potential of the ASD as an alternative tool for spectral analysis of radar signals. Fig. 4 shows the PSD (top) and lag-1 ASD (bottom) along a single azimuth for time-series data collected with the S-band, KCRI radar in Norman, OK on July 27, 2009 at the lowest elevation angle (0.5°). Data were collected using a pulse repetition time (PRT) of 1 ms ($v_a = 25$ m/s) and 41 samples and processed using a rectangular data window. Both spectral representations are plotted as a function of normalized Doppler velocity ($x$-axis) and range ($y$-axis), where the intensity of every bin represents the signal-to-noise (SNR) from $-20$ dB (light gray) to 80 dB (black). It should be noted that whereas the PSD is plotted on a normalized velocity axis given by $v_n(k) = 2k/M$, the ASD provides a more natural means of assigning normalized velocity by using the phase information as $v_n(k') = \arg[\hat{S}_l'(k')]/\pi$. To allow direct comparison of the two spectral representations, the ASD velocity axis is re-binned using the same frequency resolution as the PSD such that

$$\begin{aligned}\hat{S}_l'(k') &= \sum_{k\in B(k')} \hat{S}_l(k), \text{ where } B(k') \\ &= \left\{ k \Big| \frac{2k'-1}{M} \le \frac{\arg\left[\hat{S}_l(k)\right]}{\pi} < \frac{2k'+1}{M} \right\}, \\ 0 &\le k' < M. \end{aligned} \tag{4.10}$$

Thus, compared to the classical PSD, the ASD provides a more faithful spectral distribution of powers as a function of Doppler

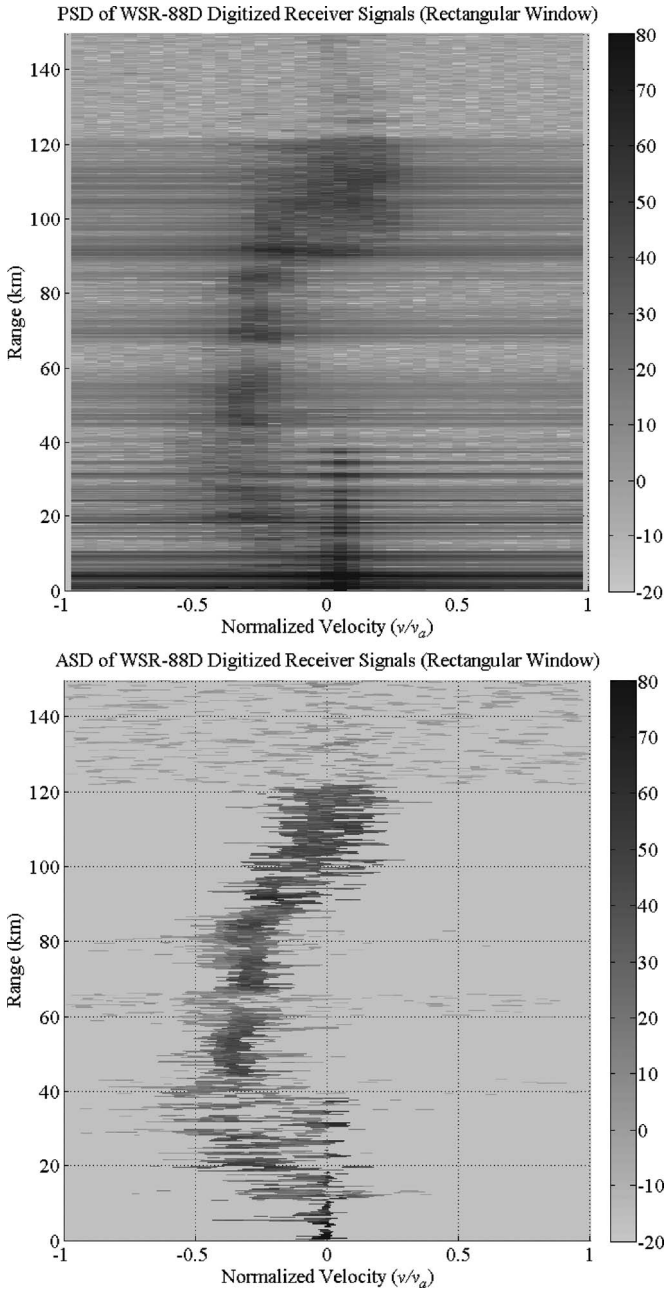


Fig. 4. PSD (top) and lag-1 ASD (bottom) as a function of normalized Doppler velocity ($x$-axis) and range ($y$-axis) for data collected with the KCRI radar in Norman, OK.

velocity because (1) bias from spectral leakage is mitigated and (2) the independent variable depends on Doppler velocity instead of being a simple index.

Focusing on the PSD, it is easy to see horizontal bands caused by spectral leakage of strong narrowband signals at various range locations either from ground clutter or narrowband weather signals (the most egregious ground clutter contamination is close to the radar from 0 to $\sim$40 km). In contrast, wideband signals have horizontal bands of lighter intensity across the spectrum. The farthest ranges ($>$ 120 km) are virtually devoid of weather signals and contain just white noise. Compared to the PSD, the ASD shows narrowband signals with narrow spectral extent and wideband signals with wide spectral extent. Although the PSD and ASD look different to the eye (this is especially evident in range locations devoid of signal), the PSD and ASD total powers for a given range location are the same (as they should be). Visual differences in plots of the PSD and ASD are expected since they are two different spectral representations (e.g., for the PSD, the $x$ axis is a mere index, while for the ASD it is a function of Doppler velocity) and should be interpreted as such. For instance, weak weather signals at about 60 km are not apparent in the PSD, but are clearly visible in the ASD. Still, other weak weather signals are obscured in both representations where there is strong ground clutter contamination since the rectangular window is used. Fortunately, this situation can be greatly improved by the use of tapered data windows, enabling the ASD as a practical tool for spectral analysis as will be illustrated next.

## V. Examples of Spectral Analysis Using the ASD

As discussed in the previous section, the phase information in the ASD can be exploited to distinguish between narrowband and wideband signals. Novel uses of the ASD at multiple lags have been suggested for ground clutter mitigation and velocity dealiasing of non-uniform sampling schemes, such as dual-polarization staggered PRT [30] and alternate dual-polarization transmission schemes [31]. In this section, two examples of the application of the lag-1 ASD for spectral analysis are presented. Although a comprehensive analysis of these applications is not covered here, the examples provide a qualitative confirmation that the additional information conveyed by the ASD can be useful in the spectral analysis of radar signals.

### A. Ground Clutter Mitigation

Using the different characteristics of ground clutter and weather signals, a novel use of the lag-1 ASD phase to automatically identify and mitigate ground-clutter contamination was introduced in [20] and comprehensively assessed and demonstrated to meet NEXRAD technical requirements in [21]. Ground-clutter returns are characterized by very narrow spectrum widths ($<$ 0.5 m/s) and zero mean Doppler velocity [4], whereas weather signals can have wider spectrum widths (the median in severe weather is between $\sim$2 to $\sim$4 m/s [19]) with velocities anywhere in the Nyquist co-interval. As seen in Section IV, the biases in the phase of the lag-1 ASD are caused by spectral leakage and respond to dominant narrowband signals in the spectrum. Thus, the behavior of narrowband signals in the lag-1 ASD can be used to recognize and mitigate ground clutter contamination.

The ground-clutter identification and filtering technique proposed in [20] relies on the phase of the ASD and is presented here to illustrate the use of the ASD in a practical application; a comprehensive evaluation of the filtering technique is beyond the scope of this work. First, the zero-frequency power level is used as a proxy for the expected ground-clutter power at each range gate. Then, the first sidelobe levels of the rectangular, Hamming, von Hann, Blackman, and Blackman-Nuttall data windows are compared against the expected ground clutter power, and the least aggressive (tapered) data window is selected so that that the expected spectral leakage from ground

clutter will be contained without unnecessarily increasing the variance of autocorrelation estimates. Typically, more aggressive windows (Blackman and Blackman-Nuttall) are selected at close ranges where ground-clutter contamination is the strongest. The lag-1 ASD of a noiseless ground clutter model (GCM) defined as a Gaussian spectrum with zero mean Doppler velocity and 0.3 m/s spectrum width [21] is used to establish the expected phase limits (i.e., the required filter notch width) for ground clutter contamination. The lag-1 ASD phases are then used to identify the spectral extent of ground clutter contamination by comparing the measured phases to the GCM phases. Filtering takes place by replacing the magnitude and phase of contaminated ASD coefficients with linearly interpolated values.

Fig. 5 shows the magnitude (top) and phase (bottom) of the lag-1 ASD as a function of the normalized velocity $v_n(k) = 2k/M$. The unfiltered (thin black line) and filtered (thick gray line) lag-1 ASD are shown for the data in Fig. 4 and radar volumes at 5 km [Fig. 5(a)], 9 km [Fig. 5(b)], and 53 km [Fig. 5(c)] in range. As described above, an appropriate data window was selected based on the expected ground-clutter power. For these examples, the Blackman-Nuttall window was selected for the first two cases (closer to the radar), whereas the Hamming window was selected for the third case (farther away from the radar).

At $\sim$5 km from the radar [Fig. 5(a)], both weather (spanning from $-0.7$ to $-0.3$; local maximum at $-0.45$ with an SNR of 34.2 dB and a phase of $-1.39$ rad) and ground clutter (spanning from $-0.2$ to 0.2; local maximum at 0 with an SNR of 65.3 dB and a phase of 0.02 rad) are observed in the unfiltered lag-1 ASD. Spectral components corresponding to a flattened phase were automatically identified as ground-clutter contaminated and are labeled with asterisks $(*)$. Two measures of filtering performance are provided: clutter suppression (the ratio of unfiltered to filtered power), and the velocity estimates before and after filtering. For this example, the unfiltered and filtered SNRs are 52.7 dB and 25.2 dB, respectively, i.e., the filter provides ground clutter suppression of 27.5 dB. Additionally, the unfiltered and filtered velocity estimates are 0.25 m/s and $-9.78$ m/s, revealing that the velocity bias due to ground clutter contamination is reduced after filtering.

At $\sim$9 km from the radar [Fig. 5(b)], ground clutter (spanning from $-0.2$ to 0.2; local maximum of 74.6 dB at 0) is observed to dominate the unfiltered lag-1 ASD. Just as in Fig. 5(a), a flattened phase (Fig. 5(b) bottom) is observed and automatically identified as ground-clutter contaminated components. The filtered lag-1 ASD shows that the ground clutter is effectively identified and mitigated. In this case, the unfiltered and filtered SNRs are 61.9 dB and 7.25 dB, respectively, so the filter provides a ground clutter suppression of 54.65 dB. Such a signal would be censored due to the amount of ground clutter contamination; therefore, velocity estimates are meaningless in this case.

At $\sim$53 km from the radar [Fig. 5(c)], a weather signal (spanning from $-0.7$ to $-0.05$; local maximum at $-0.35$ with SNR of 45.3 dB and phase of $-1.06$ rad) is observed to dominate the lag-1 ASD. No flattened phase (Fig. 5(c) bottom) is observed, so no filtering is applied.

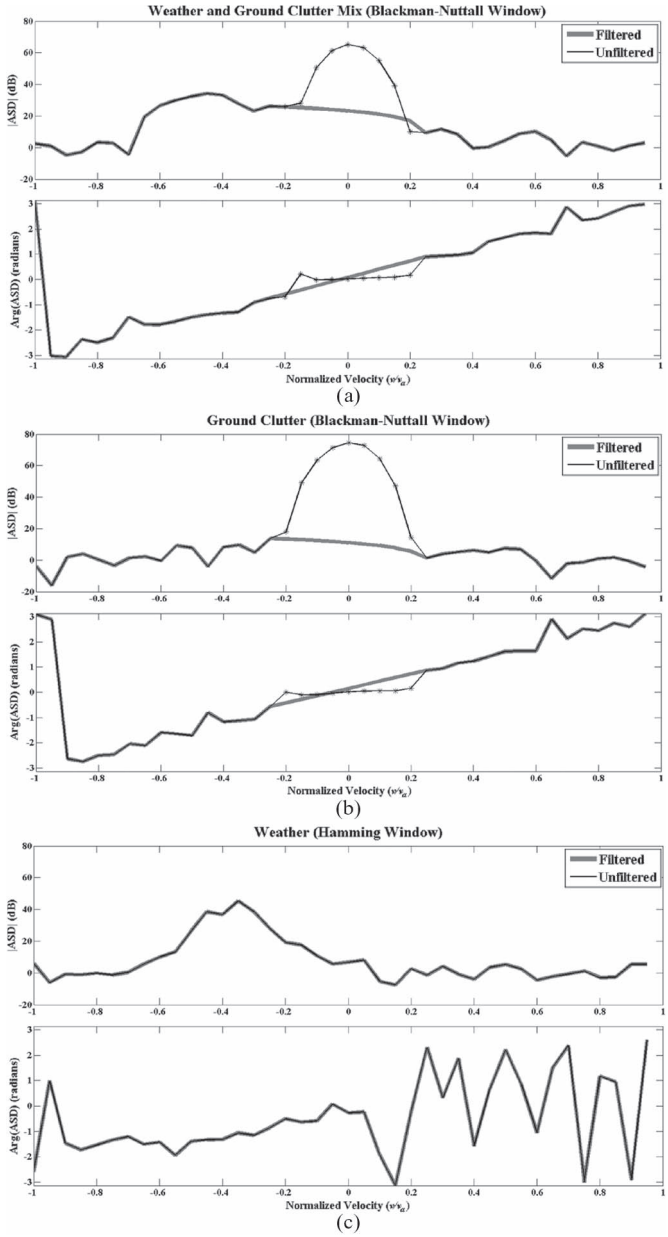


Fig. 5. (a). Magnitude (top) and phase (bottom) of the unfiltered (thin black line) and filtered (thick gray line) lag-1 ASD for weather and ground clutter mix at $\sim$5 km from the radar. Nine coefficients (denoted with asterisks) are identified as ground-clutter contaminated; these are removed and a linear interpolation is used to reconstruct the weather signal across the filter notch. Approximately, 28 dB of clutter suppression is achieved. (b). Same as Fig. 5(a), but for ground clutter at $\sim$9 km from the radar. Nine coefficients are identified as ground clutter and $\sim$55 dB of clutter suppression is achieved. (c). Same as Fig. 5(a), but for a weather return at $\sim$53 km from the radar. No ground-clutter contamination is identified and no filtering is applied.

### *B. Point Target Identification and Tracking*

Radar returns from point targets (e.g., radio towers, buildings, cars, or aircraft) are complex, aspect-angle dependent, and may exhibit motion (e.g., [22, Ch. 2 and 6]). Despite that, point targets have a small spatial extent as compared to the radar resolution volume [11]. Thus, they do not pose much of a nuisance to the quality of weather-radar-data estimates as they can be effectively mitigated with a simple range-smoothing filter (e.g., WSR-88D point-clutter rejection [23]). Still, it may

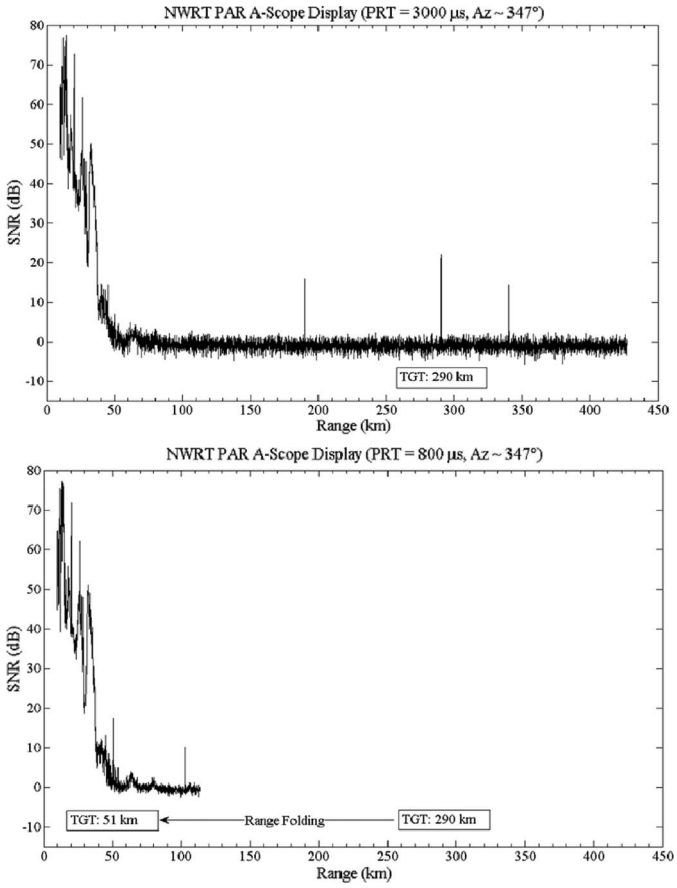


Fig. 6. Mean SNR as a function of range for long-PRT (top) and short-PRT (bottom) data collected on May 14, 2009 with the NWRT PAR in Norman, OK. A point target is shown in the long-PRT data at ∼290 km. Approximately 4.5 seconds later, the point target appears range folded in the short-PRT data at ∼51 km.

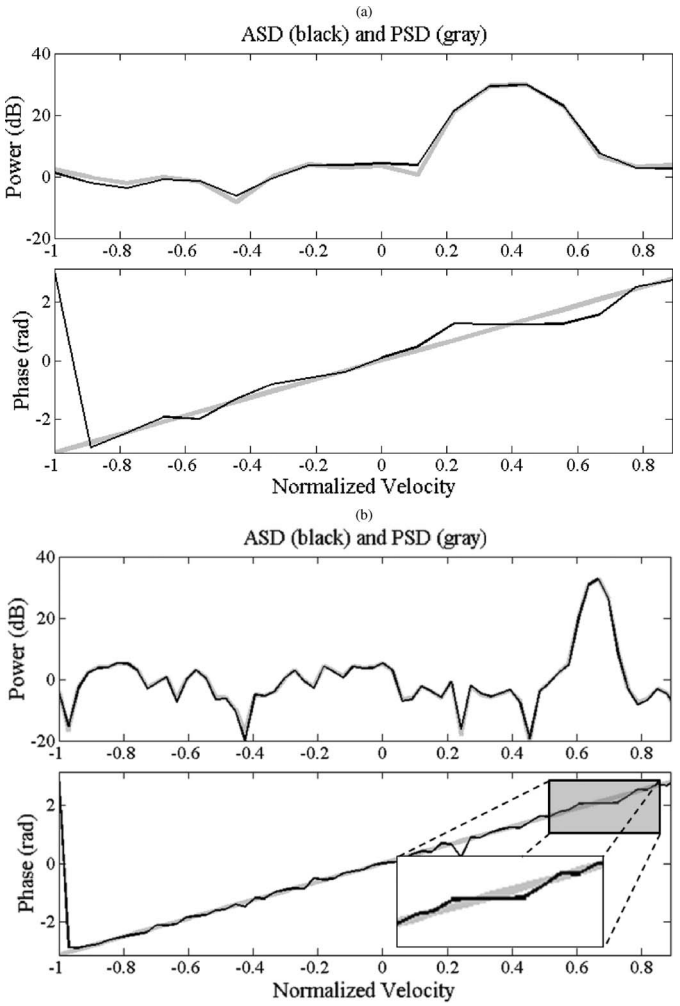


Fig. 7. Long- and short-PRT data sets corresponding to a radar volume containing a strong point target are analyzed with the PSD and ASD. For each PRT set, the top plot shows the PSD (gray) and magnitude of the lag-1 ASD (black) and the bottom plots shows the expected lag-1 ASD phase (gray) and the measured phase (black). (a) Long PRT; (b) Short PRT.

be instructive to analyze a moving point target such as an aircraft using the ASD.

For this case, we analyze digitized radar signals from the S-band, National Weather Radar Testbed (NWRT) Phased Array Radar (PAR) in Norman, OK collected on May 14, 2009 at an elevation angle of 0.5°. The mean SNR as a function of range along a single azimuth is shown in Fig. 6 (top) for a long-PRT scan (3 ms) and (bottom) for a short-PRT scan (0.8 ms). A point target is identified at 290.40 km in the long-PRT data and at 50.66 km in the short-PRT data. The short PRT has an unambiguous range $(r_a)$ of ∼119.90 km, which accounts for the apparent range reduction of the target in this scan. Although the radial velocity of this target could be estimated from the observed scan-to-scan displacement, a better estimate can be obtained from the PSD or ASD. Fig. 7 presents the PSD and the lag-1 ASD (magnitude and phase) corresponding to the long-PRT and short-PRT scans as a function of the normalized Doppler velocity for the range bins that contain the target. The expected theoretical lag-1 ASD phases are also shown. The Nyquist velocity is 7.8 m/s for the long PRT and 29.3 m/s for the short PRT, and all spectra were estimated using a Blackman window. The target is observed at ∼0.4 normalized velocity in the long-PRT spectrum, with an estimated (aliased) velocity of 3.1 m/s (18.7 m/s after dealiasing). In the short-PRT spectrum, the target is observed at ∼0.7, with an estimated velocity of 20.5 m/s. Estimated velocities using (3.2) with the ASD- and PSD-based autocorrelation estimates are within 0.01 m/s.

Although estimating the Doppler velocity of a point target is a trivial task, it is interesting to point out that the lag-1 ASD clearly shows a flattened region of phases in both the long-PRT and short-PRT spectra even though the magnitudes of the lag-1 ASD and PSD are nearly identical. As discussed in Section IV, the flattening of the phase in the lag-1 ASD is expected of signals with very narrow spectrum. Such a phase signature exhibited in the lag-1 ASD may provide a spectral analysis tool to detect and remove aircraft contaminants from weather signals while allowing aircraft tracking in a multifunctional radar system, such as the one proposed in [24] for future replacement of the WSR-88D.

## VI. Conclusion

In this paper, the autocorrelation spectral density (ASD) was introduced as a generalization of the classical periodogram-based PSD and as an alternative tool for spectral analysis of weather-radar signals. The statistical performance of the ASD estimator was shown to be comparable to that of the PSD;

however, the ASD conveys explicit phase information which reveals spectral signatures not obvious in the PSD. An ASD-based autocorrelation estimator was proposed and was shown to be equivalent to the classical time-domain, unbiased autocorrelation estimator. Thus, the ASD can be used as an alternative tool for spectral analysis of weather-radar signals where the goal is to obtain unbiased estimates of meteorological data. It was demonstrated that the biases in the phase of the lag-1 ASD of narrowband signals contrast distinctly with those of wideband signals. Hence, the ASD provides additional information not typically evident with traditional spectral analysis using the PSD. Biases in the expected linear behavior of the ASD phase can be used to recognize strong, narrowband contamination and provide an alternative approach to mitigate certain types of clutter contamination. Practical application of spectral analysis using the ASD was illustrated with ground-clutter and point-target examples. Although the practical applications presented here highlight the lag-1 ASD, the authors continue to research the applicability of other lags of the ASD in the context of non-uniform sampling schemes, such as staggered PRT. In summary, the ASD was introduced as a novel tool for spectral analysis of weather signals. It provides an alternative means for identifying strong narrowband contamination, leads to unbiased autocorrelation estimates, and has the potential to improve the quality of the meteorological data for weather radars.

## Appendix A
## Statistics of the ASD Estimator

The mean and variance of the ASD estimator defined in (2.1) are derived next. Substituting (2.3) in (2.1), the ASD estimator can be put in terms of the complex time series as

$$\hat{S}_l(f) = \frac{T_s}{M-l} \cdot \sum_{m=0}^{M-l-1} \sum_{m'=0}^{M-l-1} d(m)d(m')V^*(m)V(m'+l)e^{-j2\pi f T_s(m'-m)}. \tag{A1}$$

The expected value of (A1) is

$$E\left[\hat{S}_l(f)\right] = \frac{T_s}{M-l} \cdot \sum_{m=0}^{M-l-1} \sum_{m'=0}^{M-l-1} d(m)d(m')R(m'+l-m)e^{-j2\pi f T_s(m'-m)} \tag{A2}$$

where, the autocorrelation at lag $l$ is defined in the usual manner [11] as

$$R(l) = E\left[V^*(m)V(m+l)\right]. \tag{A3}$$

The double summation in (A2) can be re-written by collecting same-lag autocorrelation terms as

$$E\left[\hat{S}_l(f)\right] = T_s \cdot \sum_{n=-M+l+1}^{M-l-1} R(n+l)e^{-j2\pi f T_s n} \sum_{n'=0}^{M-l-|n|-1} \frac{d(n')d\left(n'+|n|\right)}{M-l} \tag{A4}$$

which is analogous to [11, (5.28)]. Further, the lag window $w$ is defined as in [11]:

$$w(n) = \begin{cases} \sum_{n'=0}^{M-l-|n|-1} \frac{d(n')d(n'+|n|)}{M-l} & |n| < M-l \\ 0 & \text{otherwise} \end{cases} \tag{A5}$$

so, (A4) can be written as

$$E\left[\hat{S}_l(f)\right] = T_s \sum_{n=-\infty}^{\infty} R(n+l)w(n)e^{-j2\pi f T_s n}. \tag{A6}$$

The sum in the previous equation can be recognized as the DTFT of the sequence $R(n+l)w(n)$, denoted as $\mathcal{F}[R(n+l)w(n)]$. Using DTFT properties [25], it can be expressed as

$$\begin{aligned} \mathcal{F}\left[R(n+l)w(n)\right] &= \mathcal{F}\left[R(n+l)\right] \circledast \mathcal{F}\left[w(n)\right] \\ &= e^{j2\pi f T_s l}\mathcal{F}\left[R(n)\right] \circledast \mathcal{F}\left[w(n)\right] \end{aligned} \tag{A7}$$

where, $\circledast$ denotes circular convolution. The PSD, denoted by $S(f)$, is defined as the Fourier transform of the autocorrelation function [26]; i.e.,

$$S(f) = T_s\mathcal{F}\left[R(n)\right]. \tag{A8}$$

Finally, introducing (A7) and (A8) in (A6), it is simple to write the expected value of the lag-$l$ ASD estimator as a function of the PSD:

$$E\left[\hat{S}_l(f)\right] = \left[S(f)e^{j2\pi f T_s l}\right] \circledast W(f) \tag{A9}$$

where, $W(f) = \mathcal{F}[w(n)]$ is real valued since $w(n)$ is an even function. Not surprisingly, if $l = 0$, the ASD becomes the PSD and (A9) becomes the well-known expected value of the periodogram estimator (e.g., [27, (10.15)]).

The mean square value of (A1) is

$$\begin{aligned} E\left[\left|\hat{S}_l(f)\right|^2\right] &= \frac{T_s^2}{(M-l)^2} \sum_m \sum_{m'} \sum_{m''} \sum_{m'''} d(m)d(m')d(m'')d(m''') \\ &\quad \cdot E\left[V^*(m)V(m'+l)V(m'')V^*(m'''+l)\right] \\ &\quad \cdot e^{-j2\pi f T_s(m'-m+m''-m''')} \end{aligned} \tag{A10}$$

where, the expected value of the quadruple product of complex time series can be decomposed using the Gaussian moment factoring theorem [28] as

$$\begin{aligned} &E\left[V^*(m)V(m'+l)V(m'')V^*(m'''+l)\right] \\ &\quad = R(m''-m)R^*(m'''-m') \\ &\qquad + R(m'+l-m)R^*(m'''+l-m''). \end{aligned} \tag{A11}$$

Thus, (A10) becomes

$$\begin{aligned} E\left[\left|\hat{S}_l(f)\right|^2\right] &= \frac{T_s^2}{(M-l)^2} \sum_m \sum_{m''} d(m)d(m'')R(m''-m) \\ &\quad \times e^{-j2\pi f T_s(m''-m)} \\ &\quad \cdot \sum_{m'} \sum_{m'''} d(m')d(m''')R^*(m'''-m') \\ &\quad \times e^{j2\pi f T_s(m'''-m')} \end{aligned}$$

$$+\frac{T_s^2}{(M-l)^2}\sum_m\sum_{m'} d(m)d(m')R(m'+l-m)\times e^{-j2\pi fT_s(m'-m)}\cdot\sum_{m''}\sum_{m'''} d(m'')d(m''')R^*(m'''+l-m'')\times e^{j2\pi fT_s(m'''-m'')} \quad \text{(A12)}$$

where, each double sum can be handled similarly to (A2) to get

$$E\left[\left|\hat{S}_l(f)\right|^2\right]=\left|T_s\sum_n R(n+l)w(n)e^{-j2\pi fT_sn}\right|^2+\left|T_s\sum_n R(n)w(n)e^{-j2\pi fT_sn}\right|^2. \quad \text{(A13)}$$

Recognizing that the first term on the right-hand side of the previous equation is the magnitude squared of (A6), the variance of (2.1) is

$$\begin{aligned}Var\left[\hat{S}_l(f)\right]&=E\left[\left|\hat{S}_l(f)\right|^2\right]-\left|E\left[\hat{S}_l(f)\right]\right|^2\\&=\left|T_s\sum_n R(n)w(n)e^{-j2\pi fT_sn}\right|^2\\&=[S(f)\circledast W(f)]^2\end{aligned} \quad \text{(A14)}$$

which can be recognized as the variance of the periodogram estimator of a Gaussian random process (cf. [29, (9.6-5)]). Thus, the variance of the ASD estimator is the same as the well-known variance of the PSD estimator.

## Appendix B
## Statistics of the ASD-Based Autocorrelation Estimator

The ASD-based autocorrelation estimator is defined as

$$\hat{R}_{ASD}(l)=\frac{1}{(M-l)T_s}\sum_{k=0}^{M-l-1}\hat{S}_l(k) \quad \text{(B1)}$$

where, the lag-$l$ ASD estimator is now more conveniently expressed in terms of discrete Fourier transforms (DFT) as

$$\hat{S}_l(k)=\frac{T_s}{M-l}F_0^*(k)F_l(k),\quad 0\le k<M-l \quad \text{(B2)}$$

where

$$F_0(k)=\sum_{m=0}^{M-l-1} d(m)V(m)e^{-j\frac{2\pi mk}{M-l}},\quad \text{and} \quad \text{(B3)}$$

$$F_l(k)=\sum_{m=0}^{M-l-1} d(m)V(m+l)e^{-j\frac{2\pi mk}{M-l}}. \quad \text{(B4)}$$

In terms of the complex time series, the ASD-based autocorrelation estimator can be written as

$$\begin{aligned}\hat{R}_{ASD}(l)&=\frac{1}{(M-l)^2}\sum_k\sum_m\sum_{m'} d(m)d(m')\cdot V^*(m)V(m'+l)e^{-j\frac{2\pi k}{M-l}(m'-m)}\\&=\frac{1}{(M-l)^2}\sum_m\sum_{m'} d(m)d(m')V^*(m)V(m'+l)\cdot\sum_k e^{-j\frac{2\pi k}{M-l}(m'-m)}\\&=\frac{1}{M-l}\sum_m d^2(m)V^*(m)V(m+l)\end{aligned} \quad \text{(B5)}$$

where, we used the fact that the sum of complex exponentials on $k$ is $(M-l)\delta(m'-m)$[25], a Kronecker delta at $m=m'$. For a rectangular data window, $d(m)=1$ for $0\le m<M-l$, and the ASD-based autocorrelation estimator is identical to the unbiased autocorrelation estimator; thus, the statistical properties of $\hat{R}_{ASD}$ are the same as those of $\hat{R}_{UNB}$, which are well understood. On the other hand, for any data window, the expected value of the ASD-based autocorrelation estimator is

$$E\left[\hat{R}_{ASD}(l)\right]=R(l)\left[\frac{1}{M-l}\sum_{m=0}^{M-l-1} d^2(m)\right]. \quad \text{(B6)}$$

Thus, the ASD-based autocorrelation estimator is unbiased only if the data window is properly scaled as a power-preserving window.

The mean square value of (B1) is

$$\begin{aligned}E\left[\left|\hat{R}_{ASD}(l)\right|^2\right]&=\frac{1}{(M-l)^2}\sum_m\sum_{m'} d^2(m)d^2(m')\cdot E\left[V^*(m)V(m+l)V(m')V^*(m'+l)\right]\\&=\frac{1}{(M-l)^2}\sum_m\sum_{m'} d^2(m)d^2(m')\cdot\left[|R(l)|^2+|R(m'-m)|^2\right]\\&=|R(l)|^2+\frac{1}{(M-l)^2}\cdot\sum_m\sum_{m'} d^2(m)d^2(m')\,|R(m'-m)|^2\end{aligned} \quad \text{(B7)}$$

where, we used the Gaussian moment factoring theorem [28] as in (A11). Thus, the variance of the ASD-based autocorrelation estimator is

$$Var\left[\hat{R}_{ASD}(l)\right]=\sum_{n=-M+l+1}^{M-l-1}|R(n)|^2\cdot\sum_{n'=0}^{M-l-|n|-1}\frac{d^2(n')d^2\,(n'+|n|)}{(M-l)^2}. \quad \text{(B8)}$$

The reader should note that for $d(m)=1$ for $0\le m<M-l$, this equation agrees with the well-known variance of the unbiased autocorrelation estimator (cf. [27, (6.63)]).

## Acknowledgment

The authors would like to thank D. Zrnić, C. Curtis, and two anonymous reviewers for providing useful comments that helped improve the quality of this paper.

## References

[1] L. H. Janssen and G. A. Van der Spek, "The shape of doppler spectra from precipitation," *IEEE Trans. Aerosp. Electron. Syst.*, vol. AES-21, no. 2, pp. 208–219, Mar. 1985.

[2] D. Zrnić, "Estimation of spectral moments for weather echoes," *IEEE Trans. Geosci. Electron.*, vol. GE-17, no. 4, pp. 113–128, Oct. 1979.
[3] D. Zrnić, "Spectrum width estimates for weather echoes," *IEEE Trans. Aerosp. Electron. Syst.*, vol. AES-15, no. 5, pp. 613–619, Sep. 1979.
[4] H. L. Groginsky and K. M. Glover, "Weather radar canceller design," in *Proc. 19th Conf. Radar Meteorol.*, Boston, MA, USA, 1980, pp. 192–197.
[5] R. E. Passarelli, P. Romanik, S. G. Geotis, and A. D. Siggia, "Ground clutter rejection in the frequency domain," in *Proc. 20th Conf. Radar Meteorol.*, Boston, MA, USA, 1981, pp. 295–300.
[6] A. Siggia and J. Passarelli, "Gaussian Model Adaptive Processing (GMAP) for improved ground clutter cancellation and moment calculation," in *Proc. 3rd ERAD*, Visby, Sweden, 2004, pp. 67–73.
[7] R. Ice, R. D. Rhoton, D. S. Saxion, C. A. Ray, N. K. Patel, D. A. Warde, A. D. Free, O. E. Boydstun, D. S. Berkowitz, J. N. Chrisman, J. C. Hubbert, C. Kessinger, M. Dixon, and S. Torres, "Optimizing clutter filtering in the WSR-88D," presented at the 23rd.Int. Conf. Interactive Information Processing Systems (IIPS) Meteorology, Oceanography, Hydrology, San Antonio, TX, USA, Jan. 14–18, 2007, Paper P2.11.
[8] S. M. Bachmann, "Phase-based clutter identification in spectra of weather radar signals," *IEEE Geosci. Remote Sens. Lett.*, vol. 5, no. 3, pp. 487–491, Jul. 2008.
[9] R. Passarelli and A. Siggia, "The autocorrelation function and Doppler spectral moments: Geometric and asymptotic interpretations," *J. Clim. Appl. Meteorol.*, vol. 22, no. 10, pp. 1776–1787, Oct. 1983.
[10] R. Doviak, D. S. Zrnic, and D. S. Sirmans, "Doppler weather radar," *Proc. IEEE*, vol. 67, no. 11, pp. 1522–1553, Nov. 1979.
[11] R. Doviak and D. Zrnić, *Doppler Radar and Weather Observations*, 2nd ed. San Diego, CA, USA: Academic, 1993.
[12] S. Torres, C. D. Curtis, D. S. Zrnić, and M. Jain, "Analysis of the new NEXRAD spectrum width estimator," presented at the AMS 33rd Conf. Radar Meteorology, Cairns, Australia, Aug. 6–10, 2007, Paper P7.8.
[13] M. H. Hayes, *Statistical Digital Signal Processing and Modeling*. New York, NY, USA: Wiley, 1996, pp. 408–412.
[14] S. M. Kay, *Fundamentals of Statistical Signal Processing, Volume I: Estimation Theory*. Englewood Cliffs, NJ, USA: Prentice-Hall, 1993.
[15] E. M. Stein and R. Shakarchi, *Fourier Analysis: An Introduction*. Princeton, NJ, USA: Princeton Univ. Press, 2003, pp. 52–54.
[16] F. Harris, "On the use of windows for harmonic analysis with the discrete Fourier transform," *Proc. IEEE*, vol. 66, no. 1, pp. 51–83, Jan. 1978.
[17] A. Nuttall, "Some windows with very good sidelobe behavior," *IEEE Trans. Acoust., Speech, Signal Process.*, vol. ASSP-29, no. 1, pp. 84–91, Feb. 1981.
[18] *WSR-88D System Specifications 2810000H*, Radar Oper. Center, Norman, OK, Apr. 25, 2008.
[19] M. Fang, R. J. Doviak, J. Richard, and V. Melnikov, "Spectrum width measured by WSR-88D: Error sources and statistics of various weather phenomena," *J. Atmos. Ocean. Technol.*, vol. 21, no. 6, pp. 888–904, Jun. 2004.
[20] D. A. Warde and S. M. Torres, "Automatic detection and removal of ground clutter contamination on weather radars," presented at the AMS 34th Conf. Radar Meteorology, Williamsburg, VA, USA, Oct. 5–9, 2009, paper P10.11.
[21] S. Torres, D. Warde, and D. Zrnić, "Signal design and processing techniques for WSR-88D ambiguity resolution: Part 15 The CLEAN-AP filter," Nat. Severe Storms Lab., Norman, OK, USA, 2012. [Online]. Available: http://cimms.ou.edu/~torres/Documents/NSSL%20Ambiguity%20Report%20-%20Part%2015.pdf
[22] M. I. Skolnik, *Introduction to Radar Systems*, 3rd ed. New York, NY, USA: McGraw-Hill, 2001, p. 772.
[23] Office Federal Coordin. Meteorol., Federal Meteorological Handbook No. 11, Part C, *WSR-88D Products and Algorithms*, Silver Spring, MD, USA, 2006. [Online]. Available: http://www.ofcm.gov/fmh11/fmh11partc/pdf/04-chap-4.pdf
[24] *Federal Research and Development Needs and Priorities for Phased Array Radar*, Office Federal Coordin. Meteorol., Silver Spring, MD, 2006, FCM-R25-2006.
[25] A. Oppenheim and R. Schafer, *Digital Signal Processing*. Englewood Cliffs, NJ, USA: Prentice-Hall, 1999, pp. 56–62.
[26] A. Papoulis and S. U. Pillai, *Probability, Random Variables and Stochastic Processes*, 4th ed. New York, NY, USA: McGraw-Hill, 2002, ch. 12, pp. 523–548.
[27] C. W. Therrien, *Discrete Random Signals and Statistical Signal Processing*. Englewood Cliffs, NJ, USA: Prentice-Hall, 1992, pp. 305–589.
[28] I. S. Reed, "On a moment theory for complex Gaussian processes," *IRE Trans. Inf. Theory*, vol. 8, no. 3, pp. 194–195, Apr. 1962.
[29] H. Stark and J. W. Woods, *Probability and Random Processes with Applications to Signal Processing*, 3rd ed. Upper Saddle River, NJ, USA: Pearson Edu., 2002, p. 613.
[30] D. A. Warde, S. M. Torres, and B. Gallardo, "Spectral processing and ground clutter mitigation for dual polarization staggered PRT signals in Doppler weather radars," presented at the 35th Conf. Radar Meteorology, Sep. 26–30, 2011, Paper P15B.1.
[31] D. A. Warde and S. M. Torres, "Automated real-time mitigation of ground clutter contamination for Dual-Polarization Doppler weather radars," presented at the 7th Eur. Conf. Radar Meteorology Hydrology, Toulouse, France, Jun. 24–29, 2012, Paper SP 200.

**David A. Warde** (M'08) received the B.S. degree (dual major) in computer science and management/computer information systems from Park University, Parkview, MO, in 2004 and Electronic/Instrument Technology A.S. degree from Excelsior College, Albany, NY, in 1997.

From 1982 to 2002, he served as an Aviation Electronics Technician with the U.S. Navy retiring ATCS (AW/NAC). From 2003 to 2008, he worked as Radar Systems Engineer support contractor for the WSR-88D Radar Operations Center, where he designed hardware upgrades to the WSR-88D test beds and provided support of signal processing enhancements to the operational system including the base moment estimators, spectral ground clutter filter, and automated ground clutter detection. In 2008, he joined the Cooperative Institute for Mesoscale Meteorological Studies at The University of Oklahoma where he currently is a Scientist/Researcher affiliated with the National Severe Storms Laboratory (NSSL). As a member of the Advanced Radar Techniques group, he conducts research and development of innovative signal-processing and adaptive sensing techniques to improve the quality, coverage, accuracy, and timeliness of meteorological products from weather radars. In addition, he is involved in the exploration and demonstration of unique capabilities offered by multifunction phased-array radar for weather observations; and the transfer of technology to existing radar systems in government, public, and private organizations.

Mr. Warde has received numerous awards throughout his career. Most recently, he received the 2011 Department of Commence Gold Medal as a member of the Radar Research and Development Division at NSSL for scientific and engineering excellence in adapting military phased array radar technology to improve U.S. weather radar capabilities.

**Sebastián M. Torres** (S'98–M'02–SM'07) received the B.S. degree from the National University of Mar del Plata, Mar del Plata, Argentina, and the M.S. and Ph.D. degrees from The University of Oklahoma, Norman, OK, in 1995, 1997, and 2001, respectively, all in electrical engineering.

From 1991 to 1996, he was a Research Associate with the Signal Processing and Measurements Laboratory at the National University of Mar del Plata, where he worked in a team of engineers and forensic anthropologists to restore and enhance fingerprint images that allowed identification of murder victims. In 1997, he joined the Cooperative Institute for Mesoscale Meteorological Studies at The University of Oklahoma where he currently is a Research Scientist affiliated with the National Severe Storms Laboratory (NSSL). As the leader of the Advanced Radar Techniques group, he conducts research and development of innovative signal-processing and adaptive sensing techniques to improve the quality, coverage, accuracy, and timeliness of meteorological products from weather radars. In addition, he is involved in the exploration and demonstration of unique capabilities offered by multifunction phased-array radar for weather observations; and the transfer of technology to existing radar systems in government, public, and private organizations.

Dr. Torres has received the 2011 Department of Commence Gold Medal as a member of the Radar Research and Development Division at NSSL for scientific and engineering excellence in adapting military phased array radar technology to improve U.S. weather radar capabilities, and the 2003–2004 Office of Oceanic and Atmospheric Research Outstanding Scientific Paper Award. Dr. Torres holds and Adjunct Faculty position in the School of Electrical and Computer Engineering, is a member of the Graduate Faculty and the Atmospheric Radar Research Center at the University of Oklahoma.